Journal of Materials Chemistry A

Accepted Manuscript

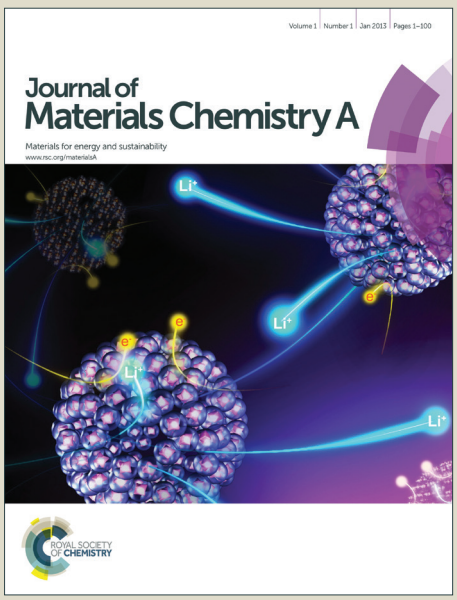

ROYAL SOCIETY OF CHEMISTRY

www.rsc.org/materialsA

Journal of Materials Chemistry A

RSCPublishing

ARTICLE

Titanium Trisulphide (TiS_3) nanoribbons for easy Hydrogen photogeneration under visible light

Cite this: DOI: 10.1039/x0xx00000x

M. Barawi, E. Flores, I. J. Ferrer, J. R. Ares, C. Sánchez

Received 00th January 2015,
Accepted 00th January 2015

DOI: 10.1039/x0xx00000x

www.rsc.org/

First evidence of hydrogen evolution by using Titanium trisulphide (TiS_3) as photoanode in a photoelectrochemical cell (PEC) is reported. Synthetized TiS_3, composed by numerous nanoribbons, has been structural, morphological and photoelectrochemically characterized. Moreover, the value of its flat band potential has been estimated (V_{fb}=-0.68±0.05V vs. Ag/AgCl) by Electrochemical Impedance Spectroscopy (EIS) measurements. This value has been used to depict the band energy levels of TiS_3/electrolyte interface. Finally, flows of photogenerated hydrogen up to 1.80±0.05 µmolH_2/min have been quantified by Mass Spectrometry (MS) at 0.3 V (Ag/AgCl) bias potential, yielding a photoconversion efficiency of about 7%.

Keywords: Metal sulphides, hydrogen photogeneration, photoelectrochemistry, solar energy conversion, solar energy chemical storage

Introduction

Energy storage directly from solar light is an attractive approach towards the need for efficient energy systems with minimal environmental impact. However, important goals need to be achieved to utilize solar energy efficiently. Collecting and storing sun energy through chemical bonds, as molecular Hydrogen, is a highly desirable methodology to solve problems related with the increasing energy demand.[1,2] There are different methods in order to achieve this aim, but water splitting cells with direct semiconductor/liquid contact are becoming a suitable option because they avoid significant fabrication costs involved in the use of electrolyzers wired to p-n junction solar cells.[3] Since Honda and Fujishima[4] discovered this phenomenon using TiO_2 more than 40 years ago, scientific community has been working to solve several problems associated with the water splitting process.

The energy conversion efficiency of solar water splitting is still low. The improvement of the efficiency relies on new materials for efficient solar energy harvesting as well as active catalysts for hydrogen and oxygen evolutions. One important step is to develop low bandgap photocatalysts. Suitable electrodes to be used in photoelectrochemical cells (PEC) for hydrogen generation should be formed by light-absorbing materials with appropriate band energy positions for the photoelectrochemical reduction of water,[5,6] i.e., bands energy levels (CB and VB) should have adequate position respect to water redox potentials.[7] To this aim, research has been shifted from single compounds (oxides, sulfides…) to new complex alternatives such as plasmonic nanostructures,[8] and two-dimensional (2D) nanomaterials.[9]

Some transition metal sulphides present advantages over these complex materials keeping the requirement of low bandgap, to absorb direct solar energy, low cost, abundant and nontoxic elements and easy synthesis process. In the last years, they have been extensively investigated for their application in Photoelectrochemical Cells (PEC). Recently, the interest in layered metal sulfides as MoS_2[10] is growing because of its low cost and excellent optical properties.

Titanium trisulphide (TiS_3) is a quasi-one dimensional sulphide that grows forming thin nanoribbons due to its linear chain type structure, in which, the chains are formed by trigonal prismatic TiS_6 units, sharing the upper and lower faces and extending

parallel to the b-axis. Its structure is monoclinic ZrSe3-type, space group P21/m[11]. TiS_3 is an n-type semiconducting material with a minimum direct optical band gap, Eg, of around 1.0 eV,[12] which has been determined by optical spectroscopy in thin films and powders.[13] A second direct energy gap has also been measured at 1.60 eV.[13] They were previously reported from photocurrent spectral response measurements.[14] Recently, their optoelectronic properties have also been investigated showing high photoresponse and electron mobility and low resistivity. These results make TiS_3 adequate to be used in applications as optoelectronics transistors.[15] Finally, TiS_3 has demonstrated to be an excellent thermoelectric material[16,17] what increases also the possibilities of being used in thermoelectric devices.

In this work, the synthesis and structural, morphological and photoelectrochemical properties of TiS_3 have been extensively investigated. Moreover, by means of Electrochemical Impedance Spectroscopy (EIS), flat band potential of TiS_3 has been determined and the energy level scheme has been established. Finally, hydrogen evolution flows have been quantified by mass spectrometry and the energy conversion efficiency has been estimated.

Experimental

Synthesis of TiS_3 Nanoribbons on Ti Substrates

Titanium trisulphide nanoribbons have been grown by titanium discs sulphuration (Goodfellow 99.9%, ∅=10mm) which had been previously etched in a HF:HNO_3 mixture (4%wt: 30%wt) to eliminate any impurities accumulated on their surfaces. Ti discs were then put into a quartz ampoule with sulphur powder (Merck, 99.75%) under vacuum (10^{-3}mb) to remove atmospheric oxygen and water and prevent oxidation of titanium during heating. Ampoules were heated with a rate of 250°C/hour and kept at 500ºC for 20 hours. (Temperatures and times of sulphuration have been previously optimized).[13,14,18]

Structural and morphological characterization

Crystal structure and crystallite size were identified by X-ray diffraction, XRD (Panalytical X'pert Pro X-ray diffractometer, CuKα radiation (λ=1.5406 Å)). Composition was analysed by Energy Dispersive X-ray, EDX (INCA x-sight). Sample´s morphology was observed using scanning electron, SEM (Oxford Instruments) and Field Emission Gun, FEG, microscopes (FEI XL-30). Electrical resistivity and Seebeck coefficient were measured by using experimental setups designed in our laboratory.[19] The BET surface area of the photocatalysts was determined by a N_2 adsorb–desorption method at −196 °C in a ASAP 2010 micrometrics equipment, using multipoint BET method at relative pressures up to 0.3. The sample was degassed before measures at 150°C under vacuum up to a lower stable value of $5x10^{-3}$ mm Hg.

Electrochemical Impedance Spectroscopy (EIS) and Hydrogen Evolution Reaction (HER)

Electrochemical measurements were performed in a three-electrode quartz cell containing an aqueous solution of 0.5M Na_2SO_3 buffered a pH=9. TiS_3 samples were used as working electrode. The counter electrode was a platinum sheet, and the reference one was an Ag/AgCl electrode. Current density (at dark and under illumination) and impedance voltage dependence were measured with a potentiostat-galvanostat PGSTAT302N provided with an integrated impedance module FRAII (10 mV of modulation amplitude is used at AC frequencies from 100Hz to 900Hz). An halogen lamp was used as visible light source. Measured light power density reaching the surface sample was 270±20mW/cm^2. This value was used to estimate the photoconversion efficiency. A Quadrupole mass spectrometer (QMS, Mod. Prisma, Balzers) coupled to the photoelectrochemical cell was used to quantify the photogenerated hydrogen. During the experiment, an argon flow of 20 sscm was passed through the top of the cell. Details are given in ref 20.

Results and Discussion

Morphological and Structural Characterization

Figure 1 shows the X-ray diffraction pattern in which TiS_3 monoclinic phase is observed as the unique crystalline phase with a preferential orientation direction probably due to the distribution of the nanoribbons. Structural parameters, obtained from the analysis of the XRD pattern, are shown in Table 1. Lattice parameters are in good agreement with those tabulated (JC-PDS 015-0783). Crystallite size (80±10 nm) has been obtained by applying Scherrer equation[21] to the (012) diffraction peak. Average of the stoichiometric ratio, determined by EDX, gives a value of S/Ti=2.9±0.1, slightly lower than expected for the stoichiometric compound.

Structural and microstructural parameters TiS3	
a (Å)	4.95±0.05
b (Å)	3.40±0.05
c (Å)	8.78±0.05
α (º)	95.45 ±0.05
$D_{(012)}$ (nm)	80 ±10

Table 1: Lattice parameters and crystallite size obtained from the XRD pattern analysis.

Nanoribbons were morphologically characterized by SEM and FEG (Fig.2). As it can be observed, TiS_3 is formed by fine and long nanoribbons which have widths between 1 and 5µm, lengths longer than 100µm, and thicknesses from 50 to 200nm. These nanostructures of Titanium sulphide give large active surface area which could improve the reaction kinetics. In order to quantify the specific area of TiS_3 nanoribbons, BET analysis was carried out. Results show a BET surface area of 67m^2/g which is really large compared with the geometrical surface

(Supporting information). Porosity has not been found in this material.

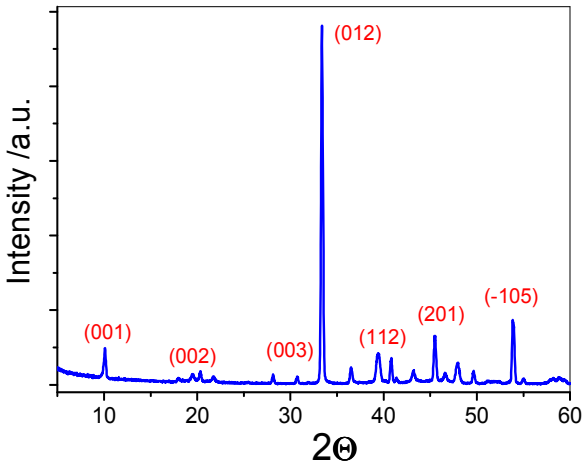

Figure 1: X- ray diffraction pattern of a TiS_3 sample grown at 500ºC during 20 hours.

Nanomorphology is an important key to obtain promising results[22] for catalytic process because of the large exposed area shown by relatively small samples. TiS_3 presents a large surface area due to its morphology of nanoribbons which grow directly from titanium substrate. It is expected that nanoribbons reduce the carrier diffusion and increase the reaction surface area, as well as improve the evolution surface kinetics. The synthesis process, which is easier and cheaper than others as electrodeposition or electrospinning[23], confers to this material an additional advantage.

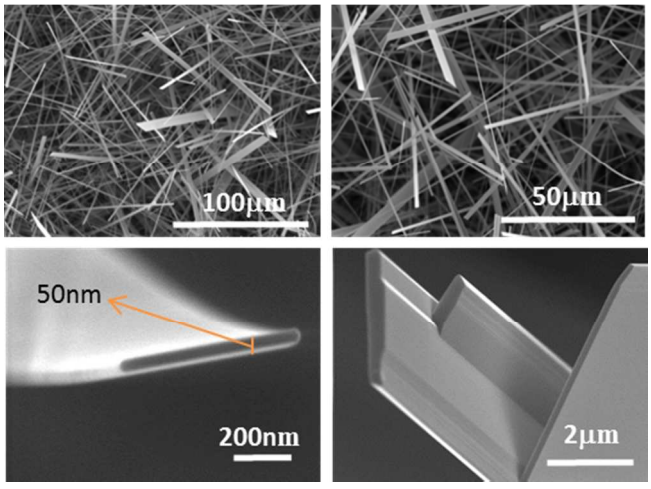

Figure 2. SEM (a, b) and FEG (c, d) images at different magnifications of TiS_3 nanoribbons grown at 500°C during 20 hours.

Photoelectrochemical activity

Dark and photocurrent densities are shown in Fig.3. Figure 3a shows the I-V curve of as prepared TiS_3 nanoribbons. Photocurrent densities of several mA have been measured. Fig. 3b shows the corresponding I-V curve of a flattened sample which shows really lower photocurrent densities (<1mA) than the as grown ones. This fact demonstrates the importance of sample morphology. In addition, a significant increase of the dark current is obtained, at a given bias potential, which could be attributed to the increased of the contact surface of TiS_3 with the metal substrate. At last, photocurrent onset potential is close to -0.1V vs. (Ag/AgCl) in both samples, before and after flattening, in good agreement with previously reported results[16]. All these effects can be seen by comparing Fig. 3a with Fig. 3b.

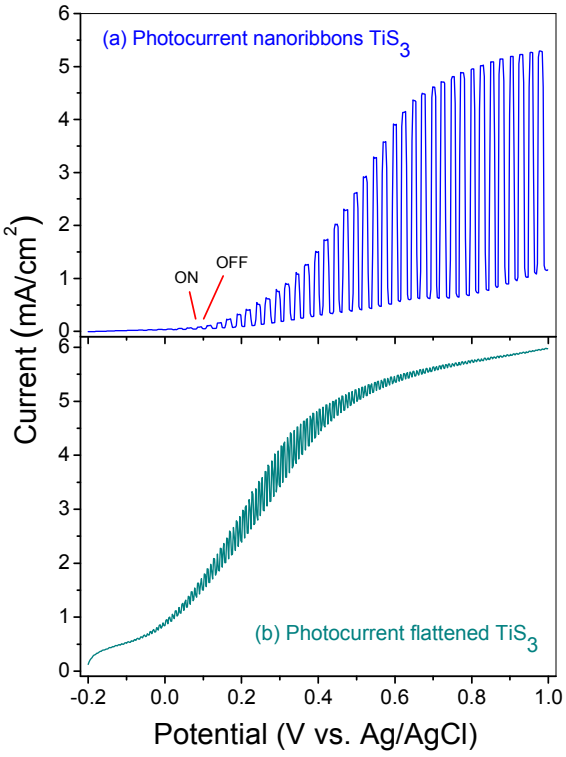

Fig3.(a) Linear sweep voltammetry of the TiS_3 nanoribbons photo-electrode under chopped white light illumination, scan rate 10 mV/s. (b) Linear sweep voltammetry of the TiS_3 flattened nanoribbons photo-electrode under same conditions than (a).

The difference in the photocurrent is accompanied by a change in the XRD pattern, as it can be seen in Figure S2 (Supporting Information), which show different relative intensities of the XRD peaks. This fact is probably due to the bending of the nanoribbons, exposing different planes to the incident x-ray. More pilled nanoribbons could reduce the active surface for the charge transfer, decreasing the photocurrent density and the light absorption. However, the effect of the crystallographic plane exposed should not be neglected. More efforts are being devoted in order to elucidate this question.

Photocurrent spectral response of TiS_3 at 0.5 V (vs. Ag/AgCl) is shown in Figure 4a, beside the corresponding Tauc plot to determine the energy band gap (Fig. 4b). Two direct transitions can be observed corresponding to E_g=1.06± 0.05eV and 1.29 ±

0.05eV. These results are in good agreement with previously reported experimental values obtained from photocurrent response[14] and optical absorption measurements[13], even though they are obtained with TiS_3 grown at 550°C.

Figure 4. (a) Photocurrent spectral response of TiS_3 in Na_2SO_3 at 0.5V (Ag/AgCl),

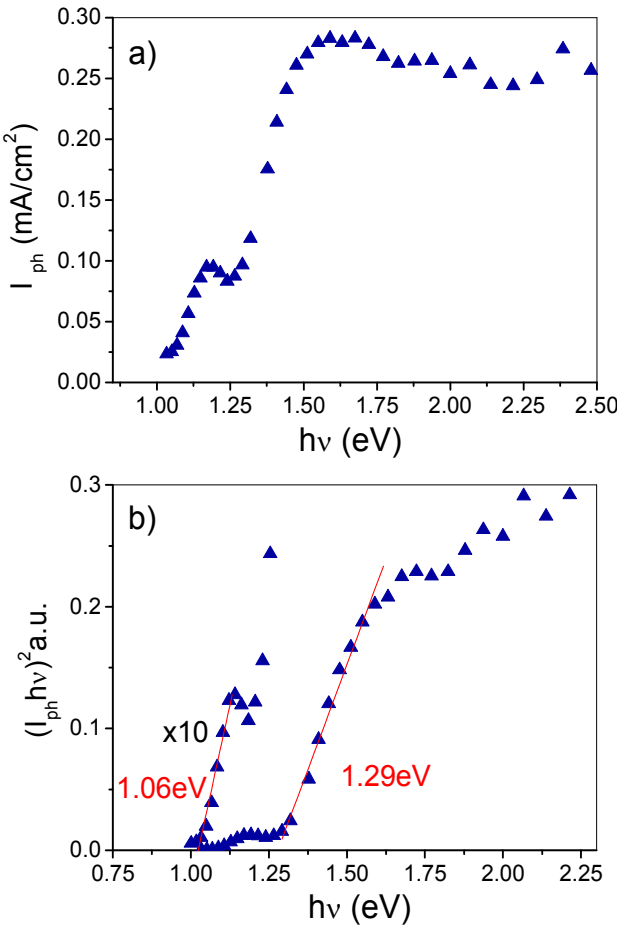

(b) Tauc plot from photocurrent shown in (a).

Flat band potential determined by EIS

Energy band edges can be experimentally estimated from the flat band potential, which is commonly determined from capacitance measurements by using the Mott-Schottky equation. V_{fb} is a property of the semiconductor/electrolyte interface, therefore, it is determined not only by the semiconductor properties but also by the electrolyte.

V_{fb} of TiS_3 has been obtained from the space charge layer capacitance (C_{SC}) measured by potentiodynamic electrochemical impedance spectroscopy, (EIS)[24]. In order to determine the space charge layer capacitance, AC modulated cyclic voltage scans from -1.0 V to 0.5V, in a range of frequencies between 100 Hz and 900 KHz, were performed, at dark conditions. The capacitance of the space charge layer is calculated by assuming

$$1/(wZ_{im}) = Csc \qquad [1]$$

where w is the frequency and $Z_{im}$is the imaginary part of the impedance.

The dependence of C_{SC} on bias potential (V) is described by the Mott-Schottky equation: [25-27]

$$\frac{1}{C_{SC}^2} = \left(\frac{2}{\varepsilon_{SC}\varepsilon_0 N_D e_0}\right)\left([V - Vfb] - \frac{k_B T}{e_0}\right) \qquad [2]$$

where C_{SC} is the measured differential capacitance per unit area, e_0 is the elementary charge, ε_{SC} is the material dielectric constant, ε_0 is the electrical permittivity of vacuum, N_D is the semiconductor donor density, V is the applied bias potential in volts, k_B is Boltzmann´s constant, and T is the measurement temperature (298K). Therefore, from the C_{SC}^{-2} vs. V plot, V_{fb} can be easily obtained by the interception with the x-axis.[25-27]

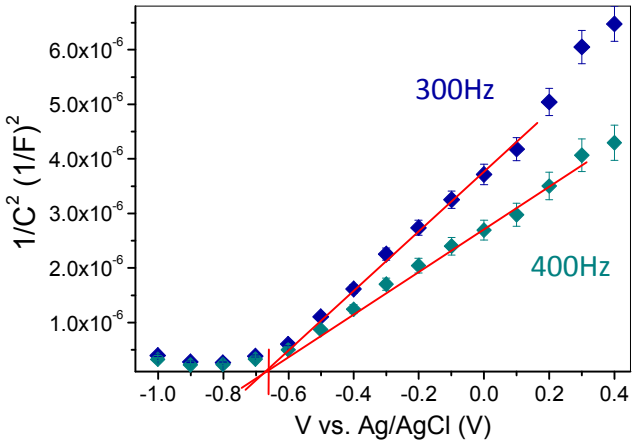

Figure 5: Mott-Schottky plot of TiS_3 in Na_2SO_3 electrolyte at pH=9 under dark conditions at AC frequencies of 300 and 400Hz.

Fig. 5 shows the Mott-Schottky plots at two frequencies and the estimated flat band potential $V_{fb} = -0.68 \pm 0.02\ V\ (Ag/ClAg) = -0.48V \pm 0.02\ V(NHE)$. The term $\left(-\frac{k_B T}{e_0}\right)$ has been neglected because of its low value.

Figure 6 presents the energy levels diagram at the TiS_3/electrolyte interface at pH=9, depicted with our

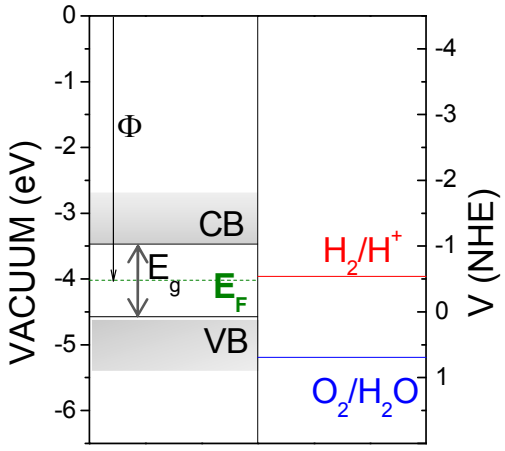

experimental data. Flat band potential ($V_{fb} = -0.48V_{NHE}$) is used to locate the semiconductor Fermi level (assuming zero charge situation). An energy band gap of E_g = 1.1eV, obtained from the photocurrent spectral response, is considered. And finally, the position of the energy Fermi level into the TiS_3 band gap, predicted by theoretical calculations[28] (0.5eV from the bottom of the CB) is taken into account. Reported value of TiS_3 work function, Φ=4.60eV[29], could also be used to determine the Fermi level energy. However, a discrepancy between the E_F energy determined from V_{fb} and that obtained from work function of about 0.6 eV exists. This discrepancy can be due to the sensitivity of the work function to chemical changes, since deviations of the order of 1 eV in the value of measured work function are common, for metals and semiconductors, depending on the surface condition.

Figure 6. Conduction and valence band energy levels in potential (V vs. NHE) and energy (eV vs. vacuum) scales. Redox potentials for the water-splitting half reactions at pH=9.0 vs. NHE are also included.

H_2 generation and Solar Energy Conversion

Figure 6 shows that, the reduction of water to generate hydrogen at the TiS_3/electrolyte could be thermodynamically possible.[25,30] The nature of evolved gases under different polarization conditions was investigated. To this aim, gas flow was analyzed "in situ" by a mass spectrometer. Flow is formed by hydrogen and no traces of oxygen are observed, confirming the band level scheme depicted in Fig.6, i.e. the reduction of water to generate hydrogen at the TiS_3/electrolyte is thermodynamically possible but oxygen generation is forbidden. This result leads to an easy implementation in a commercial device since oxygen should be removed if produced.

Figures 7a and 7b show the hydrogen photogeneration rate at 0.0 V (Ag/AgCl) and at different bias potentials, respectively, under white light illumination. As far as we know, there are not previously reported data on H_2 generation by using TiS_3 nanoribbons under visible light. As it can be observed, flow

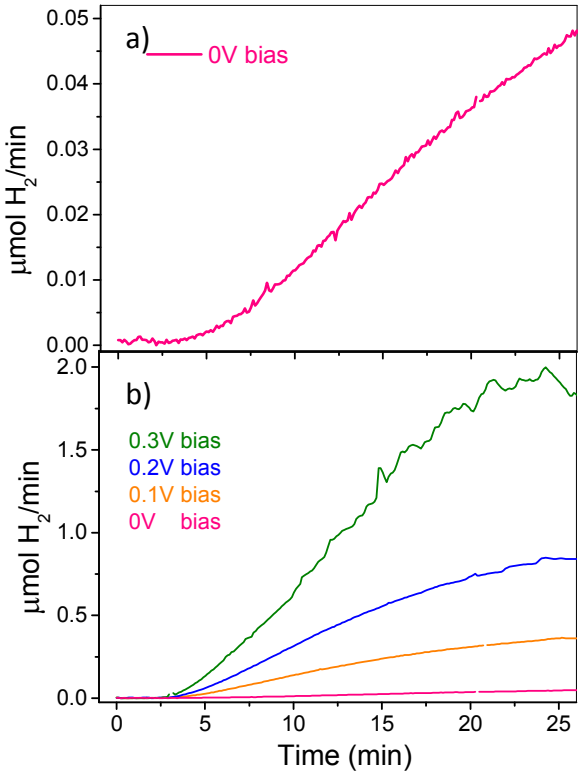

goes up as bias potential is increased, reaching values of 1.8 μmolH_2/min. at 0.3V (Ag/AgCl). **Table 2** resumes the hydrogen photogeneration rates, the total amount of hydrogen generated during 20 minutes and the photoconversion efficiency, estimated at different applied voltages by means of eq. [3] .[31,32]

Oxygen evolution is not detected by QMS, since the oxidation of water is not thermodynamically favourable, in agreement with the energy levels scheme depicted in Fig. 6. The oxidation of SO_3^{2-} to SO_4^{2-} is the alternative reaction, where SO_3^{2-} acts as a sacrificial agent. Reaction at electrodes interfaces are as follows:

- Anode: $SO_3^{2-} + 2h^+ + 2OH^+ \rightarrow SO_4^{2-} + H_2O$
- Cathode: $2H^+ + 2e^- \rightarrow H_2$

Figure 7. Hydrogen evolution flow by using TiS_3 nanoribbons: a) at 0.0 V (vs. Ag/AgCl) bias potential, b) at different bias potentials (vs. Ag/AgCl)

Results hint that a great amount of hydrogen can be obtained. H_2 flows and amounts are truly high compared with other PEC systems which need longer times to get similar amounts.[33,34]

Finally, one of the most significant parameter is the efficiency of solar energy conversion into hydrogen. Solar energy conversion efficiency may be determined by using the equation[25] [3], which is used when an external electrical bias is needed:

$$\eta = \frac{\Delta G^0_{H_2} R_{H_2} - V_b \cdot I}{P_S A} \times 100 \qquad [3]$$

where the first term accounts the chemical energy harvested by the photogenerated hydrogen, ΔG^0_{H2} (237.2kJ/mol) is the standard Gibbs energy (at 25ºC and 1 bar) of water splitting and R_{H2} is the rate of production of hydrogen (mol/s) in its standard state) per unit area of the photoelectrode, P_S is the power density of illumination in (W/m^2) (270mW/cm^2, in our measurements), A is the surface area (m^2), V_b is the external bias potential (V in volts.) and I is the current density (A) responsible for the generation of hydrogen at the rate R_{H2}, therefore, it is assumed that all the carriers contributes for generating hydrogen. In many cases[25], the efficiency is commonly overestimated because the measurements are usually performed in a three-electrode system and the bias potential used in the equation is provided by the potentiostat that should take into account the open circuit potential,[35] instead of the cell voltage, as should be used. However, here we used the approximation proposed by Liu et al.[36] to estimate the external potential imposed between TiS_3 working photoanode and the platinum counter electrode avoiding that overestimation.

Bias Potential V vs. Ag/AgCl	H2 rate (µmolH2/ min)	Total H2 in 20min (µmolH2)	Photoconversion efficiency[i] η (%) eq.[3]	Photoconversion efficiency[ii], η (%) eq. [3]
0.0	0.05± 0.05	2.4 ± 0.2	0.40 ± 0.2	0.05± 0.2
0.1	0.36± 0.05	13.0 ± 0.2	2.70 ± 0.2	0.86± 0.2
0.2	0.85± 0.05	30.9 ± 0.2	5.17 ± 0.2	0.99± 0.2
0.3	1.94± 0.05	63.5± 0.2	14.40 ± 0.2	7.30± 0.2

Table2. Hydrogen evolution rates, photogenerated hydrogen in 20 min. and photoconversion efficiency at different bias potentials.

i) Vb used in eq.[3] is estimated considering the value of the open circuit voltage, Voc.35. ii) Efficiency is estimated considering Vb as the cell potential calculated by Liu approximation 36.

Table 2 shows the photoconversion efficiency calculated using both assumptions about the applied potential, to compare their results and confirm the overestimation. Furthermore, results shown in Table 2 demonstrate the high efficiency of TiS_3 nanoribbons as a photoanode in a PEC for hydrogen generation. Compared with other materials investigated by us, such as PdS,[20] TiS_3 yields higher efficiencies in the HER process. Recalculating the efficiency of PdS by the Liu approximation [36] the efficiency of TiS_3 is 5 times higher than that of PdS at 0.3 V vs. Ag/AgCl. The total amount of photogenerated hydrogen during 20 min. is also larger (more than 20 times) than that from PdS[20].

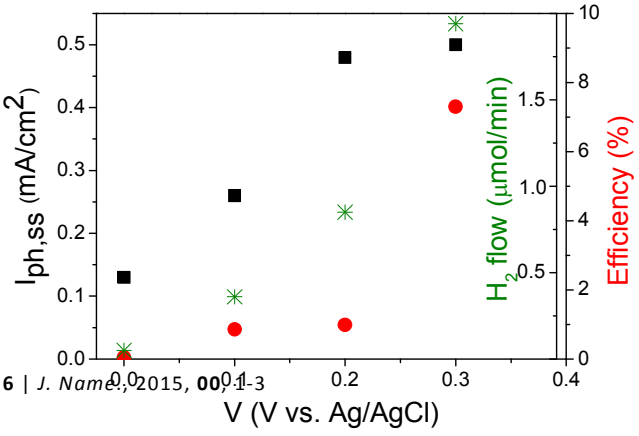

Figure 8. Steady state photocurrent density, H_2 photogenerated flow and Solar Energy Conversion Efficiency as a function of the applied potential.

Figure 8 shows the steady state photocurrent as a function of the applied potential, showing its increasing trend up to reach a saturation value at V> 0.2V (Ag/AgCl). This increasing evolution is also observed in the hydrogen flow and efficiency, but without the saturation at 0.3V (Ag/AgCl).
Finally, it is worth mentioning that the material shows also a good chemical stability, which is investigated by XRD. XRD patterns of samples, before and after measurements, do not exhibit essential differences, hinting that any chemical decomposition has not taken place. (Figure S5, S. Information).

Conclusions

Direct sulphuration of titanium discs in vacuum ampoules has been used to synthetize TiS_3 nanoribbons with a large specific area. These nanoribbons have been utilized as photoanode in a PEC. TiS_3 flat band potential was determined (V_{fb} = -0.65V vs. Ag/AgCl), for the first time, and energy band positions have been set in an energy levels diagram, resulting in a suitable position to water reduction. TiS_3 shows high photocurrents under white light illumination, as well as a really great hydrogen generation rate, which has been quantified by means of mass spectrometry. Energy photoconversion efficiencies up to 7% have been calculated. All these results make TiS_3 a good candidate to be used as photoanode in a PEC device for solar hydrogen photogeneration.

Acknowledgements

Experimental support of F. Moreno is acknowledged, as well as financial support from Spanish MINECO under contract MAT2011-22780.

Supplementary information

BET isotherm, capacitance measured by EIS at different frequencies and results of X-ray diffraction patterns of as grown TiS_3 samples, flattened and after hydrogen evolution experiments have been shown.

AUTHOR INFORMATION

Notes

Address: Dpto. de Física de Materiales, Universidad Autónoma de Madrid, 28049-Madrid (Spain)

References

1 A. J. Bard and M. A. Fox, Acc. Chem. Res., 1995, 28, 141.
2 A. Heller, Science, 1984, 223, 1141.
3 J. A. Turner, Science, 1999, 285, 687.

4 A. Fujishima and K. Honda, Nature, 1972, 238, 37.
5 L. J. Minggu, W. R. Wan Daud and M. B. Kassim, Int. J. Hydrog. Energy, 2010, 35, 5233.
6 H. O. Finklea, J. Chem. Educ., 1983, 60, 325.
7 X. Chen, S. Shen, L. Guo and S. S. Mao, Chem. Rev., 2010, 110, 6503.
8 S. Mubeen, J. Lee, N. Singh, S. Krämer, G. D. Stucky and M. Moskovits, Nat. Nanotechnol., 2013, 8, 247.
9 T.-F. Yeh, C.-Y. Teng, S.-J. Chen and H. Teng, Adv. Mater., 2014, 26, 3297.
10 L. Gao, Y. Cui, J. Wang, A. Cavalli, A. Standing, T. T. T. Vu, M. A. Verheijen, J. E. M. Haverkort, E. P. A. M. Bakkers and P. H. L. Notten, Nano Lett., 2014, 14, 3715.
11 S. Furuseth, L. Brattås, A. Kjekshus, A. F. Andresen and P. Fischer, Acta Chem. Scand., 1975, 29a, 623.
12 H. G. Grimmeiss, A. Rabenau, H. Hahn and P. Ness, Z. Für Elektrochem. Berichte Bunsenges. Für Phys. Chem., 1961, 65, 776.
13 I. J. Ferrer, J. R. Ares, J. M. Clamagirand, M. Barawi, C. Sánchez, Thin Solid Films 2013, 535, 398.
14 I. J Ferrer, M. D. Maciá, V.Carcelén, J. R. Ares, C. Sánchez, Energy Procedia 2012, 22, 48.
15 J. O. Island, M. Buscema, M. Barawi, J. M. Clamagirand, J. R. Ares, C. Sánchez, I. J. Ferrer, G. A. Steele, H. S. J. van der Zant and A. Castellanos-Gomez, *Adv. Opt. Mater.*, 2014, **2**, 641.
16 J.M Clamagirand, J. R. Ares, M. Barawi, I. J. Ferrer and C. Sánchez, *Proceedings from the 31st International & 10th European Conference on thermoelectrics, ICT&ECT*. Aalborg, Dinamarca, 2012.
17 E. Finkman and B. Fisher, *Solid State Commun.*, 1984, **50**, 25.
18 I.J. Ferrer, J.R. Ares, P. Díaz-Chao, C. Sánchez, *Proceedings from NanoSMat-07*. Algarve, Portugal 2007.
19 J. R. Ares, M. León, N. M. Arozamena, J. Sánchez-Páramo, P. Celis, I. J. Ferrer and C. Sánchez, *J. Phys. Condens. Matter*, 1998, **10**, 4281
20 M. Barawi, I. J. Ferrer, J. R. Ares and C. Sánchez, *Appl. Mater Interfaces*, 2014, **6,** 20544.
21 L.V. Azaroff, *Elements of X-ray Crystallography*, McGraw Hill, Tokyo, 1968.
22 M. Zhou, X. W. (David) Lou and Y. Xie, *Nano Today*, 2013, **8**, 598.
23 H. Hou, L. Wang, F. Gao, G. Wei, J. Zheng, B. Tang and W. Yang, *Int. J. Hydrog. Energy*, 2014, **39**, 6837.
24 M. E. Orazem, *Electrochemical Impedance Spectroscopy*, John Wiley & Sons, 2008.
25 C. Grimes, O. Varghese and S. Ranjan, *Light, Water, Hydrogen: The Solar Generation of Hydrogen by Water Photoelectrolysis*, Springer, New York, 2008 edition, 2007
26 J. M Bolts, M. S. Wrighton, *J. Phys. Chem.* 1976, **80**, 2641.
27 A. S. Bondarenko, G. A. Ragoisha, *J. Solid State Electrochem.* 2005, **9**, 845.
28. J. O. Island, M. Barawi, R. Biele, A. Almazán, J.M. Clamagirand, J.R. Ares, C. Sánchez, G.A. Steele, H. S.J. van der Zant, J.V. Alvarez, R. D'Agosta, I. J. Ferrer, A.Castellanos-Gomez. Adv. Mater. In press, 2015.
29 X. C. Wu, Y. R. Tao and Q. X. Gao, *Nano Res.*, 2010, **2**, 558.
30 K. Rajeshwar, S. Licht, R. McConnell, *Solar Hydrogen Generation: Toward a Renewable Energy Future*; Springer. New York, 2008.
31 B. Parkinson, *Acc. Chem. Res.*, 1984, **17**, 431.
32 A. Iwase and A. Kudo, *J. Mater. Chem.*, 2010, **20**, 7536.
33 X. Zhang, Y. Sun, X. Cui and Z. Jiang, *Int. J. Hydrog. Energy*, 2012, **37**, 811.
34 G. Wang, H. Wang, Y. Ling, Y. Tang, X. Yang, R. C. Fitzmorris, C. Wang, J. Z. Zhang and Y. Li, *Nano Lett.*, 2011, **11**, 3026.
35 M. G.Walter, E. L.Warren, J. R. McKone, S. W. Boettcher, Q. Mi, E. A. Santori, Lewis, *Chem. Rev.* 2010, **110**, 6446.
36 M. Liu, N. de L. Snapp and H. Park, *Chem. Sci.*, 2010, **2**, 80–87.